ELSEVIER

Journal of Nuclear Materials 266–269 (1999) 666–672

journal of nuclear materials

MARFE feedback experiments on TEXTOR-94

U. Samm [a,d,*], M. Brix [a,d], F. Durodié [b,d], M. Lehnen [a,d], A. Pospieszczyk [a,d], J. Rapp [a,d], G. Sergienko [c,d], B. Schweer [a,d], M.Z. Tokar [a,d], B. Unterberg [a,d]

[a] *Institut für Plasmaphysik, Forschungszentrum Jülich GmbH, EURATOM association, 52425 Jülich, Germany*
[b] *Ecole Royale Militaire/Koninklijke Militaire School, association EURATOM-Belgian State, Brussels, Belgium*
[c] *Institute for High Temperatures IVTAN, Moscow, Russian Federation*
[d] *Members of the Filateral Euregio Center*

Abstract

This paper reports about the latest developments on feedback control of MARFEs in TEXTOR-94. This technique allows us to avoid most of the density limit disruptions and provides means to create stationary MARFEs. The best signal for MARFE detection is the CII or CIII line radiation from the vicinity of the inner wall. This signal has been used successfully in various feedback loops acting on the deuterium gas flow, the external heating power, impurity injection or the horizontal plasma position or a combination of these. The results demonstrate that the proximity to the inner wall can be of major importance for the MARFE development, quite comparable to the average electron density or the plasma current. Recombination becomes significant inside the MARFE at electron densities of about 3×10^{14} cm^{-3} and temperatures of a few eV as is shown by spectroscopy.

Keywords: MARFE; TEXTOR; Recycling; Recombination; Radiation

1. Introduction

A MARFE is a radiative instability effect, identified first in the tokamak ALCATOR C [1,2], where this name has been coined, and observed later on many other machines [3]. This instability starts when the derivative of the local radiation losses P_L with the local electron temperature T_e is negative $\delta P_L / \delta T_e < 0$ and its absolute value becomes larger than the change in heat flow into this region. This condition can be met at rather low T_e and is generally achieved first on the high field side of a tokamak, where the radial heat transport has a minimum. At this location a rather thin toroidal belt of low T_e and high electron density n_e with strong radiation develops, which typically covers about 10% of the poloidal circumference and 5–10 cm of the minor radius in the vicinity of the last closed flux surface (LCFS). Poloidal asymmetries in transport (e.g. drifts, plasma rotation, etc.) may cause the MARFE to start somewhat below or above the horizontal midplane and furthermore may lead to a slow movement of the MARFE in poloidal direction.

MARFEs are an issue for fusion machines since the operation at high densities and high radiation level is a typical regime where MARFEs are often observed. The so called divertor detachment, an important scenario for energy exhaust, is also linked to MARFEs.

Improved knowledge about the MARFE development and the conditions for MARFE onset may help to understand partly the density limit in a tokamak. Lipschultz [3] formulated a condition for MARFE onset

$$\rho = \overline{n}_e / I_p \pi a^2, \tag{1}$$

with $\overline{n}_e$ the line averaged electron density in (10^{20} m^{-3}), I_p the plasma current in mA and the minor radius a in m. In the data set available at that time MARFEs have been observed for $\rho = 0.4$–0.7 and the upper limit for the density was at $\rho \approx 1$. Later this scaling with $\rho = 1$ has been applied successfully to fit the density limit also of elongated and diverted plasmas leading to the so called Greenwald limit [4].

* Corresponding author. Tel.: +49-2461 61 3085; fax: +49-2461 61 5452; e-mail: u.samm@fz-juelich.de.

0022-3115/99/$ – see front matter
PII: S0022-3115(98)00516-9

Recently it has been shown on TEXTOR-94 that this limit can be overcome by up to a factor of 2 if one chooses conditions where the onset of MARFEs is suppressed or delayed [5]. In these experiments the *proximity* to the inner wall plays a crucial role, a parameter which is not included in Eq. (1) and is so far also not considered in MARFE theories [6–8], except a new approach developed by one of us [9]. The experimental evidence for this will be elucidated further in this paper.

A safe operation close to or with these instabilities requires the employment of feedback systems. Experiments with feedback systems may also help to identify and study the relevant mechanisms for MARFE development. We have already reported earlier about the effect of horizontal plasma positioning on MARFE development in TEXTOR [10]. On ASDEX-U it has been shown that MARFEs can be controlled with a feedback system based on bremsstrahlung and neutral beam heating [11].

In this paper we report about the latest developments on feedback control of MARFEs in TEXTOR-94. This new technique allows to avoid most of the density limit disruptions and provides means to create stationary MARFEs. By employing this technique we will demonstrate the relevance of proximity to the inner wall, the development of different types of MARFEs and present spectroscopic data from which local plasma parameters inside the MARFE can be derived.

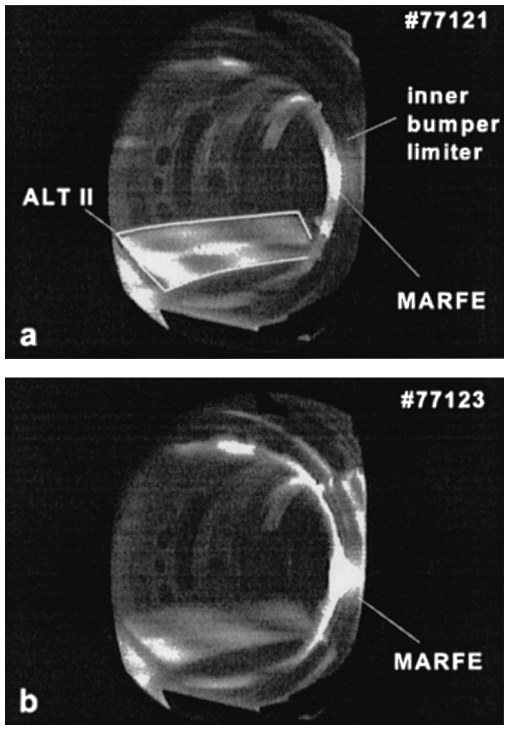

Fig. 1. Poloidal cross section of TEXTOR in the light of D_α showing MARFEs at the high field side; (a) thin MARFE when distance to inner wall is enhanced; (b) fat MARFE.

2. MARFE detection

MARFEs can be observed with all diagnostics which are sensitive to density, temperature or radiation changes at the high field side close to the LCFS. Examples exist for bolometry, interferometry, electron cyclotron emission and emission spectroscopy. The MARFE structure is most clearly seen in the poloidal cross section. Fig. 1 displays video images obtained from a CCD camera. Most of the light detected comes from D_α and some impurity lines, like carbon CII and CIII. Two types of MARFEs are shown: a 'fat' and a 'thin' MARFE, the appearance of which depends on the horizontal plasma position as is discussed later. The MARFE onset can also occur somewhat below or above midplane (±45°). Furthermore the MARFE can move poloidally. Therefore, the observation volume for MARFE detection has been choosen to be rather large as is depicted in Fig. 2.

On TEXTOR-94 we employ a filter-diode system which provides a fast signal (10 kHz) from various lines. Furthermore, a spectrometer with a tangential view is used, which allows the determination of radial emission profiles across the MARFE region (50 Hz resolution) and another spectrometer viewing radially to the in-

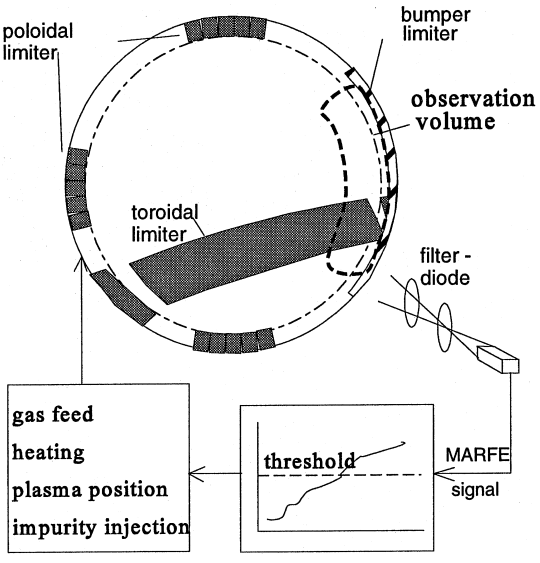

Fig. 2. Observation volume in the poloidal plane which has been used for spectroscopic MARFE detection and feed-back control.

board side and scanning via a technique with oscillating mirrors gives data for higher ionization states (e.g. CIV and CV). The most pronounced signal is obtained from CII and CIII, whose peak values rise typically by a factor of 10 with a MARFE. The higher states like CIV and CV increase much less. This has also been reported from other tokamaks (e.g. JET [12]).

We report here only about feedback control systems in which the CII radiation has been used for MARFE detection. Since the signal is averaged over a large area it may vary less than the peak values mentioned above. These peak values have been derived from emission profiles, but are so far not available online, thus cannot be used for feedback control.

3. MARFE onset and development

Among the experimental observations which lead to the development of a MARFE the most important ones are: (a) increase of density beyond a critical value, (b) increase of radiation by impurity injection, (c) decrease of heating power and (d) increase of local recycling by shifting the plasma towards the inner bumper limiter. From this list we can immediately see by which means a MARFE control should be possible. This is discussed in Section 4.

The standard case for a MARFE development is a density increase as is shown in Fig. 3. Above a critical density the MARFE starts. Fast D_α measurements show a rise time of about 2–3 ms. The line emission from carbon rises as the MARFE grows further with a characteristic time of about 12 ms. This is in agreement with the ionization and excitation times for the lower ionization states of carbon: before the MARFE in an edge plasma with $T_e \approx 50$ eV and $n_e \approx 7 \times 10^{12}$ cm^{-3} (at LCFS) the radiation from CIII builds up in about 0.1 ms, but as the plasma cools down to a few eV inside the MARFE this characteristic time rises by about two orders of magnitude.

The local cooling leads to a pressure drop which causes the MARFE to act like a pump with the result that a high local electron density of about 3×10^{14} cm^{-3} builds up. Simultaneously the line averaged central density decreases by about 10–15% as can be seen in Fig. 3. The number of electrons collected inside the MARFE volume is estimated to be about 3×10^{19}, which is consistent with the corresponding loss in the bulk plasma. In contrast to Fig. 3(a) the decrease of $\bar{n}_e$ in Fig. 3(b) coincides also with a switch off of the deuterium gas puff due to the feedback loop. From the comparison of the two curves we see that the dominating effect of density decrease is due to the pump effect in the MARFE and not to the gas injection. The gas feed applied in Fig. 3(a) leads to a growth of the MARFE and ends with a major disruption.

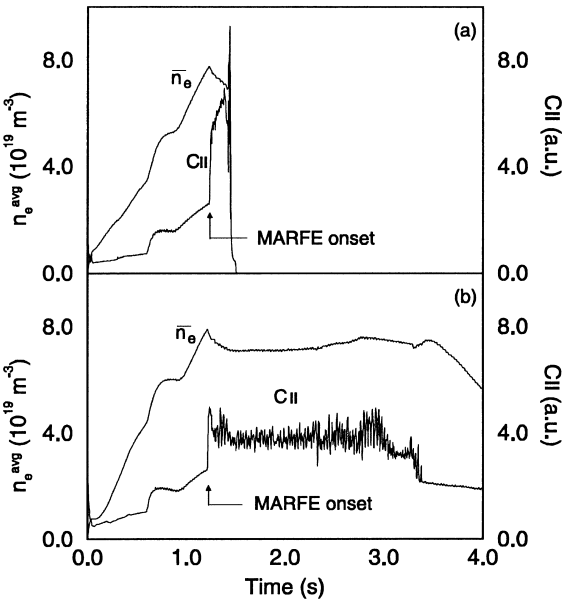

Fig. 3. Time trace of line averaged central electron density and CII line radiation from the MARFE region for (a) a discharge with density ramp until a major disruption occurs and (b) a case where the feedback system keeps the MARFE constant via an adequate gas puff control ($I_p = 450$ kA, $P_{heat} = 1.6$ MW).

In Fig. 4 time traces of $\bar{n}_e$ are shown for various horizontal plasma positions with which the distance of the LCFS to the inner bumper limiter is varied from 2.3 cm to about 6.1 cm. The critical line averaged density for MARFE onset varies from $\bar{n}_e = 4.9 \times 10^{13}$ cm^{-3} to $\bar{n}_e = 6.3 \times 10^{13}$ cm^{-3}. The shift in plasma position is linked to a change of the minor plasma radius of about

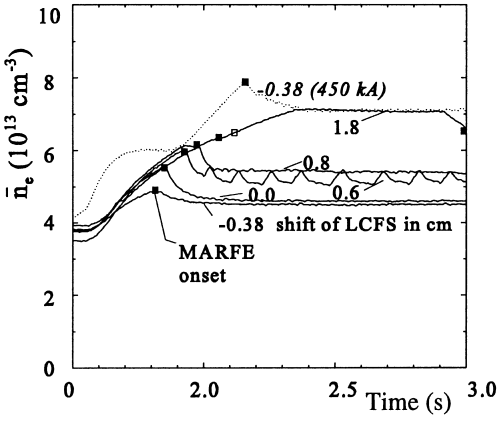

Fig. 4. Evolution of the line average density for various horizontal plasma positions. Indicated are relative shifts of the plasma column with respect to the standard position (negative/positive = inboard/outboard), which correspond to distances of the LCFS to the inner bumper limiter between 2.5 cm and 5.5 cm ($I_p = 350$ KA, $P_{heat} = 1.6$ MW).

3%. According to Eq. (1) we would expect then a change in the critical density of about 7%: i.e. an increase to $\overline{n}_e = 5.2 \times 10^{13}$ cm^{-3} rather than to $\overline{n}_e = 6.3 \times 10^{13}$ cm^{-3}. This demonstrates that the proximity to the inner wall is also a very important parameter. However, the important role of the plasma current I_p follows almost exactly the scaling: the critical density at $I_p = 450$ kA for a shift of the LCFS of 0.9 cm inboard is a factor 1.26 higher than the one at $I_p = 350$ kA with a comparable shift (0.8 cm).

The size of the MARFE depends also strongly on the distance of the LCFS to the inner wall. We observe two different types of MARFEs: a fat MARFE [Fig. 1(b)] for a short distance (<5 cm) and a thin MARFE (Fig. 1(a)) for a larger distance (>5 cm). Their properties and impact on global parameters are quite distinct.

From the region of the fat MARFE about 40% of the total radiated power P_{rad} is emitted (Fig. 5). The global radiation level P_{rad}/P_{heat} is in these cases $\gamma = 75\%$. Strong recycling on the inner wall is evident from the enhanced D_α light. A further growth of the MARFE, e.g. by strong gas puffing, would increase the radiation level to $\gamma = 100\%$ followed by a major disruption. The fraction radiated from the MARFE stays always below 50% of P_{rad}. The radial profile of CII emission shown in Fig. 6 shows that the peak radiation coincides approximately with the LCFS.

The thin MARFE radiates only 10–20% of P_{rad}. Also the CII line emission is compared to the fat MARFE about a factor of 3 less intense (Fig. 6). The D_α emission shown in Fig. 1(a) corresponds to the beginning of the MARFE development. When increasing the density further, as is seen in Fig. 4, the MARFE moves poloidally to a position about 45° below the midplane. There the radiation from the MARFE is reduced by about a factor of 3 compared to the MARFE onset. The absence of a density drop manifests that the pump effect of a thin MARFE is significantly weaker. A very important fact is

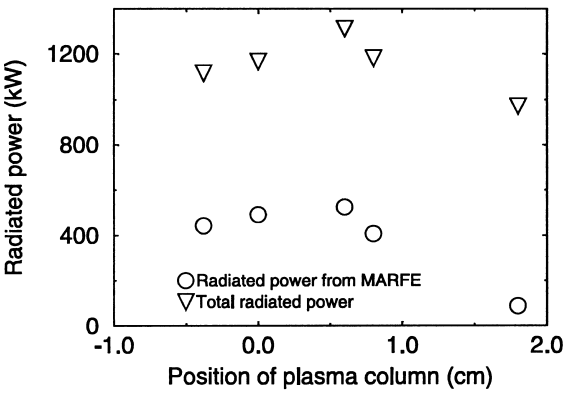

Fig. 5. Power radiated from MARFE and total power as a function of the horizontal plasma position relative to the normal position (neg. = inboard, $P_{heat} = 1.6$ MW).

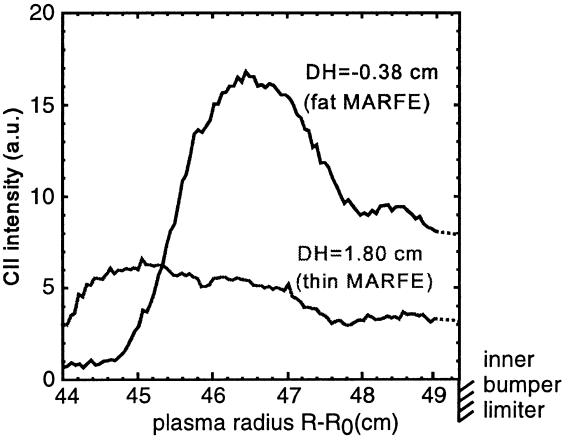

Fig. 6. Radial profile of CII line radiation in a fat and a thin MARFE; the position of the LCFS is approximately at $r = 46.9$ cm (fat) and $r = 43.3$ cm (thin).

that $\overline{n}_e$ can be increased much beyond the critical density for MARFE onset. It has been shown that under similar conditions with an optimized geometry (enhanced distance to inner wall) the Greenwald density can be overcome by up to a factor of 2 [5].

In Table 1 the line averaged central electron density $\overline{n}_e$ and edge density n_e measured by beam emission spectroscopy [13] at the low field side before and during the MARFE are given for the discharges with various plasma positions as discussed above. Also here we see that the thin MARFE ($\Delta = 6.1$ cm) has nearly no effect, neither on the central density nor on the edge plasma. In contrast, the fat MARFEs lead to a decrease of central density and edge density (pump effect), where the drop at the edge is generally more pronounced (peaking). For the strongly oscillating case two values are given (min/max).

The local densities and temperatures inside the MARFE deviate from those in a normal edge plasma, such that the standard edge diagnostics on TEXTOR-94, like atomic beams, fail to provide data. We have derived the electron density from the Stark broadening of deuterium lines [14]. Figs. 7 and 8 show spectroscopic data obtained from the vicinity of the inner wall similar to the geometry shown in Fig. 2. In Fig. 7 the line intensities before the MARFE are also shown together with the data during the MARFE.

The different increase in D_α and D_γ radiation indicates already that recombination processes begin to play a role inside MARFEs. Recombination changes the population of higher levels ($n = 5$) more than the lower ones ($n = 3$) in contrast to what one would expect from excitation due to electron impact only. This is even more pronounced from Fig. 8 where also the radiation from the levels $n = 9$,10 and 11 is seen. The increase of the various line radiation of the Balmer series is given in Table 2.

Table 1
Line averaged central electron density $\overline{n}_e$ and edge density n_e at the low field side varying with the distance of the LCFS to the inner wall Δ. The inner bumper limiter is located at $r = 49.3$ cm

Δ cm	$\overline{n}_e$ 10^{13} cm^{-3}			$n_{e\,LCFS}$ 10^{12} cm^{-3}		
	Before MARFE	In MARFE	Ratio	Before MARFE	In MARFE	Ratio
2.4	4.9	4.6	0.94	5.1	4.0	0.78
3.0	5.5	4.7	0.86	6.5	4.5	0.69
4.0	6.0	5.1/5.4	0.90/0.85	7.0	4.3	0.61
4.4	6.1	5.5	0.95	7.8	5.1	0.65
6.1	6.3	7.2	1.0	6.0	5.7	0.95

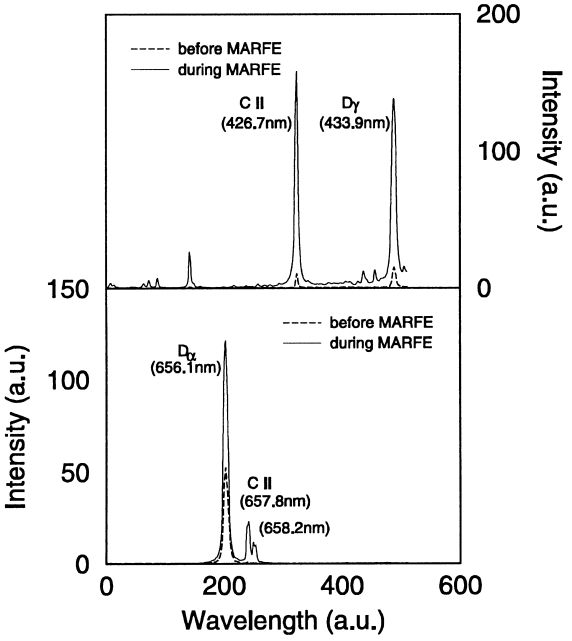

Fig. 7. Line radiation from the MARFE region. Shown are data before and during the MARFE for CII, D_α and D_γ.

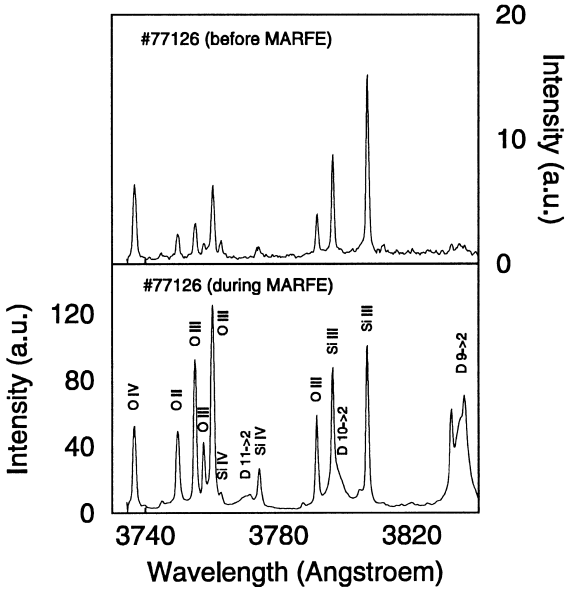

Fig. 8. Line radiation from the MARFE region which includes also hydrogen lines for high excitation levels. The transition $11 \rightarrow 2$ is used to derive n_e from Stark broadening.

We conclude that recombination is significant and is nearly as strong as it has been observed in the divertor of ALCATOR C-mod at detachment [15,16], where 50% of all ions flowing into this region recombine. The Stark broadening has been analyzed from the least disturbed lines D(11–2). We obtain values up to 3×10^{14} cm^{-3} electron density inside the MARFE. The electron temperatures are estimated to be several eV. Assuming pressure balance we obtain 2 eV.

4. MARFE feedback

The feedback scheme used on TEXTOR-94 is depicted in Fig. 2. A CII signal obtained from the high field side is compared to a preset value. If the signal is above this threshold the system (a) switches off the deuterium gas puff or (b) increases the auxilliary heating power (ICRH) or (c) switches off impurity injection or (d) moves the plasma away from the inner wall. If the signal falls back below the threshold the actions are reversed. Also combinations of these measures have been realized.

Table 2
Relative increase of Balmer lines at the MARFE onset as expected from 100% recombination (10^{15} cm^{-3}, 1 eV) [15] and the measured values normalized to $D(3 \rightarrow 2)$

Transition	Enhancement expected	Enhancement measured
$D(3 \rightarrow 2)$	2	2
$D(5 \rightarrow 2)$	15	8
$D(9 \rightarrow 2)$	600	65
$D(11 \rightarrow 2)$	1800	–

All these schemes work in principle and allow to inhibit the MARFE growth. The impurity injection method is the one with the lowest sensitivity and should normally be combined with one of the others. Plasma position feedback is rather unfavorable for experiments: the system tends to strong oscillations of the horizontal plasma position. Gas puff switch off with and without additional ICR heating turns out to give the best results. The neutral beam heating has not been integrated in the feedback loop so far. Since the strongest effect in the feedback loop comes from the deuterium gas feed, we will show in the following examples only cases where the gas feed method has been applied. In Fig. 9 two cases are shown for two different plasma positions leading to a quite distinct behaviour.

The most quiet one is obtained with a position closest to the inner bumper limiter [Fig. 9(a)]. The amplitude varies only by about 5% during feedback. The MARFE sits 'quietly' at the midplane for more than 1.5 s. The other example is a case with the most violent oscillations (Fig. 9(b)). The MARFE appears and disappears with a period of about 110 ms (compared to 40 ms in case (a)). The CII signals varies by a factor of 2. The rise time of the MARFE signal of about 12 ms is the same in both cases although the amplitudes are quite different. This agrees with the characteristic ionization times for carbon up to C^{2+}. The strong oscillation in case (b) can partly be understood from the better pumping efficiency which allows to reduce the density faster (Fig. 4), since this is the case where the plasma is shifted more to the outside where the pump limiter ALT-II is located. But the pronounced growth of the MARFE in case (b) is not yet understood.

When shifting the plasma further to the outside the tendency of the system to oscillate disappears, the MARFEs become weaker. At a distance of the LCFS to the inner wall larger than 5 cm, where the thin MARFE develops, the CII signal obtained from the filter-diode system is so small (due to averaging over a large area) that it stays below the threshold for feedback and the gas feed is not switched off. However, this case allows us to go to much higher densities without getting a disruption.

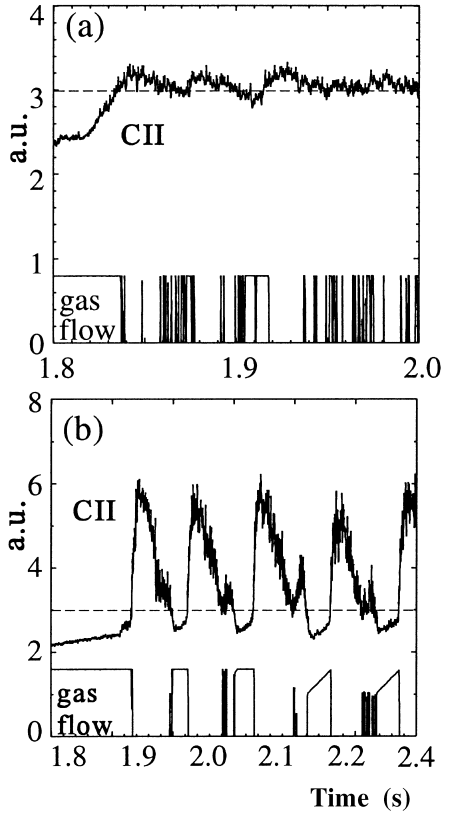

Fig. 9. MARFE feedback: shown is the signal CII and the gas flow of D_2, with the threshold for feedback preset to 3 V (a.u.) and two different horizontal plasma positions where the LCFS has a distance to the inner bumper limiter of (a) 2.5 cm and (b) 5.5 cm.

5. Discussion and conclusions

Feedback systems allow a safe operation close to the density limit. Best results have been obtained with systems based on line radiation from the MARFE zone (e.g. CII) and controlled gas puffing. The local recycling on the inner wall plays an important role in the dynamics of the feedback loop.

We have presented evidence that proximity to the inner wall is an issue for the onset of MARFEs. The distance to the inner wall or the local recycling there has been neglected so far in MARFE theories and in scalings. However, the strong sensitivity on average density and plasma current according to the Lipschultz scaling has been confirmed.

Energy losses from hydrogen alone might be sufficient for a MARFE to develop. The theoretical approach [9] to describe this instability is based on the local cooling by ionization of recycling neutrals which leads to an increase of plasma density through the pressure equilibration on magnetic surfaces. This results in a larger outflow of charged particles perpendicular to the field towards the inner wall causing the recycling to increase further. The measured rise time of 2–3 ms for the MARFE onset agrees with this theory. However, impurity radiation contributes also to the MARFE growth, leading to rise times which can be linked to the ionization times of the lower states (10–15 ms) and will also depend on the MARFE growth which may occur on a slower scale.

A large distance of the LCFS from the inner wall is favorable to obtain a high density limit. Under these conditions only thin MARFEs develop, which allow to

increase the average central density much beyond the Greenwald density. In contrast, fat MARFEs with strong local recycling at the inner wall inhibit a further increase of central density due to their strong pumping effect. Further gas puffing leads to a growth of these MARFEs and normally a major disruption follows. We have shown that fat MARFEs can be generated and kept constant during the flat top.

Strong recombination inside the MARFE has the effect of a virtual limiter in case of a fat MARFE. A large fraction of the ions recombines in the MARFE zone as if a toroidal belt limiter would have been introduced at the high field side. Most of the power flowing into the MARFE is lost in its vicinity. Further investigations are needed to decide whether this might lead to a possible application.

Acknowledgements

The TEXTOR-94 team is gratefully acknowledged for providing excellent experimental conditions. In particular the efficient help obtained from H.T. Lambertz and P. Hüttemann for setting up the feedback electronics is appreciated.

References

[1] J.L. Terry et al., Bull. Am. Phys. Soc. 26 (1981) 886.
[2] B. Lipschultz et al., Nucl. Fusion 24 (1984) 8.
[3] B. Lipschultz et al., J. Nucl. Mater. 145–147 (1987) 15.
[4] M. Greenwald et al., Nucl. Fusion 28 (1988) 2199.
[5] P.C. de Vries et al., Phys. Rev. Lett. 80 (1998) 16.
[6] J.C. Wesson, T.C. Hender, Nucl. Fus. 33 (1993) 1019.
[7] H. Kastelewicz et al., MPI report IPP 8/3 (1994).
[8] W.M. Stacey, Plasma Phys. Contr. Fusion 39 (1997) 1245.
[9] M.Z. Tokar et al., these Proceedings.
[10] U. Samm et al., in: Proceedings of 18th European Conference on Controlled Fusion and Plasma Physics, Berlin, 1991, Europhysics Abstracts, vol. 3, p. 137.
[11] K.-H. Steuer et al., in: Proceedings of 19th European Conference on Controlled Fusion and Plasma Physics, Innsbruck, 1992, Europhysics Abstracts, vol. 2, p. 743.
[12] J. O'Rourke et al., in: Proceedings of 18th European Conference on Controlled Fusion and Plasma Physics, Budapest, 1985, Europhysics Abstracts, vol. 1, p. 155.
[13] B. Schweer et al., these Proceedings.
[14] H.R. Griem, Plasma Spectroscopy, McGraw-Hill, New York, 1964, p. 92.
[15] J.L. Terry et al., in: Proceedings of 24th Europ. Conf. on Contr. Fusion and Plasma Physics, Berchtesgaden, 1997, Europhysics Abstracts, vol. 2, p. 573.
[16] J.L. Terry et al., these Proceedings.